Chemical Engineering Journal 467 (2023) 143350

Contents lists available at ScienceDirect

Chemical Engineering Journal

journal homepage: www.elsevier.com/locate/cej

Synthesis of PEG-PPG-PEG templated polydopamine nanoparticles under intensified conditions: Kinetics investigation, continuous process design and demonstration for photothermal application

Georgios Gkogkos [a], Luca Panariello [a], Eleni Grammenou [a], Mabel A. Cornwell [a], Amir Afrashtehpour [b], Alexander J. MacRobert [b], Ivan P. Parkin [c], Asterios Gavriilidis [a,*]

[a] Department of Chemical Engineering, University College London, Torrington Place, London WC1E 7JE, UK
[b] Division of Surgery and Interventional Science, University College London, Royal Free Campus, London NW3 2PS, UK
[c] Department of Chemistry, University College London, 20 Gordon Street, London WC1H 0AJ, UK

ARTICLE INFO

Keywords:
Polydopamine
Pluronic P-123
Nanoparticles
Templating
Kinetics
Millifluidics
Membrane reactor
Photothermal heating

ABSTRACT

Polydopamine is a nature inspired functional material with promising applications in a plethora of fields due to its structural, chemical, and optical properties. While there is significant interest in the preparation of polydopamine based nanomaterials that take advantage of its properties, less attention has been given to the optimisation of the synthetic process, which typically involves the oxidative self-polymerisation of dopamine under basic pH and requires 24–72 h for reaction completion. The present work investigated the kinetics of polydopamine formation in the presence of Pluronic P-123 (PEG-PPG-PEG) micelles acting as a soft template, in low monomer concentrations (that promote particle growth instead of nucleation) as a function of temperature and pressure. Simultaneous increase of pressure and temperature (up to 50 °C and 5 bar O_2) was found to significantly reduce the reaction time to 20–40 min without compromising the particle quality. Based on the results of the kinetic investigation, the polydopamine synthesis was translated into a continuous process utilising a millifluidic co-axial membrane reactor with a focus on ease of use, process conditions' reproducibility and safety of operation. The reactor produced nanoparticles similar to the batch synthesis and resisted fouling (which is generally expected in a compact flow reactor) due to the action of the P-123 surfactant. Due to the nontoxic process that utilises only biocompatible materials and oxygen as the oxidising agent, and the melanin-like structure of polydopamine, photothermal heating of the synthesised nanoparticles under concentrated IR irradiation at 808 nm light was studied, as this can potentially be used for photo-induced hyperthermia. The hyperthermia threshold of 10 °C temperature increase at relatively low laser power settings (fluence 1.77 W/cm^2) was achieved, making it a promising candidate for this application.

1. Introduction

Originally inspired by the structure of proteins found in the byssus of mussels which enables their attachment on solid surfaces even under aquatic and saline conditions [1], and exhibiting a plethora of desirable properties, polydopamine (PDA) is increasingly in the spotlight for use in the production of functional materials [2]. PDA-based materials, endowed with many of the chemical, optical and photothermal properties of PDA, have found their way in applications within a wide range of sectors including biomedicine [3-6], (photo)catalysis [7,8] and energy [9,10]. Since most of PDA properties are dependent on its structural and chemical characteristics, a lot of work has been devoted in investigating how polydopamine forms, and how to control its synthesis [11-13].

The mechanism of polydopamine formation has not been entirely understood and is possibly dependent on the substrate where PDA coatings attach and the reactive conditions. It is commonly agreed that it starts with the oxidation of dopamine and, through a series of additional oxidation, cyclisation and isomerisation steps, leads to dihydroxyindole and indole-quinone molecules that can form oligomers which eventually aggregate via hydrogen bonding, π–π interactions or additional covalent bonds [1,14]. These steps can take place simultaneously allowing the

* Corresponding author.
E-mail address: a.gavriilidis@ucl.ac.uk (A. Gavriilidis).

https://doi.org/10.1016/j.cej.2023.143350
Received 2 February 2023; Received in revised form 23 April 2023; Accepted 2 May 2023
Available online 5 May 2023

incorporation of reaction intermediates in the final polydopamine structure and leading eventually to a highly disordered material [1,15-18]. The reaction cascade can be easily performed under mildly alkaline pH (pH > 8) and ambient conditions. This approach, albeit simple to implement, offers limited control on the polydopamine formation steps and usually requires over 24 h to reach completion, which has led to investigation of various modifications to improve deposition times and control of the particle size. Thus, various approaches have been employed to accelerate polydopamine synthesis and control the structure (and consequently the properties) of the resulting material.

As a result of its disordered structure and abundance of active groups, it has been shown that PDA attaches to a wide range of substrates, including colloidal nanoparticles. Thus, PDA nanoparticle formation can be effectively directed using colloidal hard and soft templating, as demonstrated with the use of silica and carbon nanoparticles [19,20], carbon dots [21], carbon nanotubes [22], ionic surfactants [23] and block copolymers micelles loaded with 1,3,5-trimethylbenzene (TMB) [20,24,25]. To accelerate polydopamine formation, the use of strong chemical oxidants [16,26], horseradish peroxidase [27] and the Fenton system [28] have been investigated with promising results. However, these solutions offer limited particle size control (especially at sizes < 100 nm), increase the risk of oxidative degradation of produced polydopamine and may also be incorporated in the final structure of polydopamine as contaminants. Dissolved oxygen remains an important oxidant for oxidation reactions as it is abundant, environmentally benign and, due to its gaseous nature, it allows increasing its concentration by means of pressurisation to significantly accelerate the reaction. Moreover, it can be quickly separated to prevent degradation of the product. Although challenging to achieve, it has been shown that increasing the concentration of oxygen can accelerate polydopamine formation [29]. Finally, energy input by means of heating [30], UV radiation [31,32], microwave [33] and ultrasound [34], has been shown to accelerate polydopamine deposition in various substrates and thus could be also effective in accelerating polydopamine nanoparticle formation or nanoparticle surface coating.

This work utilises the principles described above for the design of an intensified process for oxygen-induced, size-controlled, polydopamine nanoparticle synthesis. It starts with investigating the templating action of a micelle-forming non-ionic surfactant and then systematically evaluates the effect of oxygen concentration in combination with the process temperature at the optimal pH range to drastically reduce the reaction time, while keeping control of the particle size. The kinetic data collected from the first part of this study are subsequently used to design a continuous production process using a co-axial membrane millifluidic reactor [35,36] that enables safer and more efficient handling of gaseous oxygen, while accelerating heat and mass transfer due to its sub-mm characteristic dimensions. The photothermal properties of the nanoparticles produced with the intensified process are further tested under a clinically relevant 808 nm NIR laser irradiation to demonstrate their potential application in photothermal cancer therapy.

2. Materials and methods

2.1. Chemicals

The dopamine solution was prepared by dissolving 3-hydroxytyramine hydrochloride (dopamine hydrochloride, Acros Organics) in DI water in a concentration of 20 mg/ml. DI water was purged with nitrogen for 1 h to prevent uncontrolled dopamine oxidation. For the preparation of the buffered micellar solution, 125.0 mg Pluronic P-123 (PEG-PPG-PEG block copolymer, MW = 5800 g/mol) and 30.3 mg of Tris.HCl (both from Sigma Aldrich) were dissolved in 25 ml DI water (~10 mM Tris and ~ 0.86 mM P-123) unless stated otherwise. HCl 1 M (Fluka) was subsequently added in the solution to tune the pH to the desired value. Concentrated NaOH 2 M (Fluka) was used directly for removing polydopamine coatings from reactor walls and components when necessary. Oxygen 99.9995% (BOC) was the oxidizing agent. Nitrogen 99.9995% (BOC) was used for purging oxygen and as the working fluid in the flow reactor pressurization (see section 2.3). Isopropanol (IPA) 99.9% (Sigma Aldrich) was used to facilitate polydopamine nanoparticle preparation for solid state analysis (e.g., FTIR).

2.2. Pressurised batch reactor for kinetic experiments

Reactor components

A thick wall, round bottom, glass pressure vessel from Chemglass™ (CG-1880-R-02, 68 ml maximum capacity) was used as the pressurised batch reactor. The vessel included a threaded PTFE cap and a Viton O-ring that provided sealing during operation. The PTFE cap was customised with the addition of two ports that connected the internal volume with external tubing. Port 1 was connected to an oxygen cylinder through an electronic mass flow controller (MFC) (BROOKS, SLA5800S,) to monitor and control the oxygen flowrate and a spring-operated back pressure regulator (BPR) (Swagelok, K-series, oil-free, 10 bar maximum pressure) that enabled a constant pressurised oxygen atmosphere during the reactor operation. An electronic pressure sensor (Druck, DPI-104) was connected to the gas line in parallel with the reactor to monitor the pressure in the reactor vessel. In Port 2, a PTFE capillary with 1.6 mm outer diameter (OD) and 0.5 mm inner diameter (ID) was inserted through the cap, with its outlet submerged in the reactive mixture. The inlet was connected to two ETFE millifluidic shut-off valves (IDEX, 1 mm ID when fully open) that allowed reactant addition and sampling, while keeping the system pressurised. The valves were connected to each other via PTFE capillary sections with 1.6 mm OD, 0.5 mm ID and PEEK fittings from IDEX. An oval shaped, PTFE coated magnetic stirrer bar was inserted in the reactor before use. Temperature control of the reactor was achieved by partially submerging it into a stirred water bath. A hot plate (Stuart, CB162) provided the heat and the magnetic stirring power for both the heating fluid and the reactor. A temperature controller connected to the hotplate monitored and controlled the heating fluid temperature via a submerged thermocouple. A schematic of the batch reactor setup can be found in SI, section S1.

Reactor operation and sample collection

For all batch experiments, the reactor was filled with 25 ml of the buffered micellar solution (P-123 and Tris.HCl in water). It was pressurised and heated to the desired conditions and was kept under stirring for ~ 60 min before addition of the dopamine solution to allow temperature equilibration between the heating fluid and the reactor contents and adequate oxygen dissolution (preliminary data had shown larger discrepancies when lower waiting times were used before the experiments).

Reactant addition in a pressurised reactor involved multiple steps: a plastic 2.4 ml syringe filled with 1 ml of the dopamine solution and 1.4 ml air, was connected vertically (liquid phase downward) at the Port 2 capillary inlet (post-mixing dopamine concentration of 5 mM or 0.769 mg/ml). The valve towards the pressurised reactor was opened, allowing a pressurisation of the small volume between the valves, and then closed to isolate this section. Subsequently, the valve towards the inlet was opened allowing the syringe to match the pressure of the reactor without compromising the reactor pressurisation (pressure equilibration sequence). The use of a small diameter syringe allowed equilibration of the pressure with a handheld syringe. The second valve was opened to connect the pressurised syringe to the reactor and add the reactant: pressing the syringe, dopamine was added in the solution, and the small amount of air in the syringe pushed any residue of the dopamine solution in the reactive mixture. This ensured consistency in dopamine concentration and cleared the capillaries to prevent contamination of the samples. Finally, both valves were closed and the syringe was disconnected. The final volume of the batch is 26 ml.

Samples from the pressurised reactor were obtained by connecting an empty syringe in Port 2, and slowly opening both valves, first the one at the reactor side. Sample volume was controlled manually via the syringe. After the sample was transferred in a vial for post processing, the capillary at Port 2 was cleared of fluid using a second air filled syringe and following the pressure equilibration sequence. A sample slightly larger than required was collected (~0.3 ml) and then a 0.2 ml sample volume was accurately measured with a pipette and diluted 10x with water. The sampling process, while complicated and time consuming (requiring 20–30 s), allowed acquisition of kinetic information from the pressurised batch process.

Testing of the reactant addition and sampling procedures showed a pressure change < 0.1 bar during operation at 5 bar. Up to 5 bar, the syringe pressure could be successfully matched manually, but the method could be used at even higher pressures by utilising a syringe pump.

2.3. Millifluidic membrane reactor

For the continuous polydopamine synthesis process, a millifluidic coaxial capillary membrane reactor was used. The system consisted of a preheating section followed by a pre-saturation section that set the reaction conditions before the dopamine addition to promote rapid dopamine oxidation; a microfluidic (0.5 mm ID) T-mixer enabled fast mixing of dopamine solution with the O_2 saturated buffer solution. A second membrane section kept the oxygen pressure constant to provide the necessary oxygen for subsequent oxidation steps required for polydopamine synthesis. An oxygen permeable Teflon AF2400 tubular membrane (Biogeneral) was used as the inner capillary, both in the pre-saturation and the reaction stages, while an 1/8 in. OD (3.175 mm) 2.4 mm ID PTFE tube around the membrane was used in a dead-end configuration to contain the gaseous oxygen atmosphere. The liquid phase pressure was controlled via a gas (nitrogen) operated back pressure regulator (Zaiput). The oxygen supply configuration was equivalent to the one used in batch synthesis and consisted of the same components (MFC, BPR and pressure sensor). The reactants were supplied continuously in the reactor via syringe pumps (Harvard, PHD2000) using a 50 ml glass syringe for the micellar buffer (SGE) and a 5 ml glass syringe (SGE) for the dopamine solution. The reactants were mixed in flow using a 0.5 mm ID PEEK T-junction (IDEX). A pressure relief valve rated for 100 psi (IDEX, U456,) was connected after the buffer solution syringe as a safety measure. A schematic of the membrane reactor system along with a photograph of the reactor are shown in SI, section S1.

2.4. Characterisation techniques

UV–Vis absorption spectra of nanoparticle samples were obtained with a QE-Pro spectrophotometer (Ocean Optics) using a deuterium-halogen light source (Ocean Optics, DH-2000-BAL) and 1.5 ml capacity single-use methacrylate cuvettes (Fisherbrand). The samples were diluted to a final 10% v/v with DI water before measurement to avoid supersaturation. Dynamic light scattering (DLS) analysis was performed with a DelsaMax Pro analyser (Beckman Coulter), diluting the original sample with DI water (to 1/20th of the initial concentration) to avoid multiparticle scattering effects. Mean particle hydrodynamic diameter and polydispersity index were obtained via cumulative analysis (assuming normal distribution), while particle size distributions were obtained via regularisation analysis. For FTIR analysis, an IRTracer-100 (Shimadzu, UK) with a diamond ATR accessory was used (Specac, Quest Single Reflection ATR). The polydopamine particles were precipitated by diluting a small amount of the sample in IPA (5% v/v dilution) and allowing it to settle. The clear supernatant was then removed with a pipette and the particles were dried overnight in a fume cupboard resulting in a thick paste. Raman spectra of polydopamine samples were obtained with a MarqMetrix All-In-One Raman System using a 798 nm laser excitation source, by pipetting 1 ml of sample in a cylindrical (ID = 15 mm), aluminium sample holder and placing the probe ~ 3 mm from the liquid surface. TEM images were obtained with a JEM 2200-FS microscope (JEOL) and analysed with ImageJ (ca. 120 particles) to obtain the particle size distribution.

2.5. Measurement of photothermal heating of nanoparticle dispersions

An NIR laser at 808 nm was used (Diomed 25) as a light source for heating experiments. 1 ml of the as-prepared nanoparticle dispersion in DI water was placed in a 10 mm optical path, square, quartz cuvette (Hellma) and a PTFE coated magnetic stirring bar was placed inside the cuvette. The laser beam was guided via a 0.4 mm core optical fibre, with the output beam aligned orthogonally to the cuvette surface at a height above the stirrer. The cuvette and the fibre were fixed in a 3D printed holder produced in-house with a Form 3 3D printer and high temperature resin (Formlabs). The distance between the fibre end and the cuvette was set at 2 mm. Using an NIR sensitive upconversion card the incident laser beam was visualised for verifying that the beam would only pass through the liquid within the cuvette. A slot in the cuvette holder accommodated a thin thermocouple (Picotechnology, model TC-08), so that it was in direct contact with the outside of the cuvette; it was placed parallel to the laser beam (thus not directly illuminated by the laser), below the sample surface. Temperature measurements were acquired at 10 Hz and logged via PicoLog™ software. The cuvette was capped during the heating measurements to prevent solvent evaporation, reducing heat loss and ensuring a constant sample concentration during the measurement. The fibre-cuvette holder was placed on a magnetic stirrer with the stirring speed set at 500 rpm. In all measurements the laser was set at its minimum power (0.5 W) illuminating a small circular area of the cuvette surface (fluence of 1.77 W/cm^2).

3. Results and discussion

3.1. Effect of Pluronic P-123 on polydopamine synthesis

P-123 is a water-soluble triblock copolymer consisting of alternate poly(ethylene glycol) (PEG) and poly(propylene glycol) (PPG) blocks in a PEG_{20}-PPG_{70}-PEG_{20} sequence. In an aqueous environment it forms micelles when in concentrations above 0.313 mM or 1.815 mg/ml, which is its critical micelle concentration (CMC) [37]. The more hydrophobic PPG part forms the micelle core while the hydrophilic PEG chains are in contact with the water. It has been proposed that catechol and amine groups found in most polydopamine structural blocks may interact with the ether oxygen atoms of PEG chains via hydrogen bonding, and this interaction eventually leads to the formation of smaller aggregates [38]. P-123 has been used, in combination with Pluronic F-127 to form micelles encapsulating hydrophobic TMB, as a templating agent for shape-controlled PDA synthesis [25]. In addition, PDA formation in the presence of various surfactants has been shown to control PDA particle size by encapsulation of PDA nanoparticles in micelles [23]. This approach also prevented deposition of PDA on solid surfaces, which is highly desirable in the context of continuous flow synthesis. Similar interactions could be expected for P-123 surfactant, which would allow P-123 micelles to act as a soft template.

A series of experiments were performed to verify the above hypothesis. PDA synthesis was performed at ambient conditions (~20 °C, air atmosphere) for 24 h in the presence of P-123 at different concentrations and the size (hydrodynamic diameter, D_H) and polydispersity (polydispersity index, PDI) were measured by DLS (see Fig. 1). For P-123 concentrations above the CMC, the micelle size (measured via DLS) was 22–30 nm, slightly decreasing with increasing concentration. Polydopamine nanoparticles synthesised in the presence of Pluronic P-123 micelles (P-123@PDA NPs) were found to be larger by approximately 10 nm compared to the original micelles (as seen in Fig. 1, for samples S3, S4 and S5), while maintaining a similarly low polydispersity index (PDI ≤ 0.1). In the absence of P-123, >200 nm nanoparticles were produced,

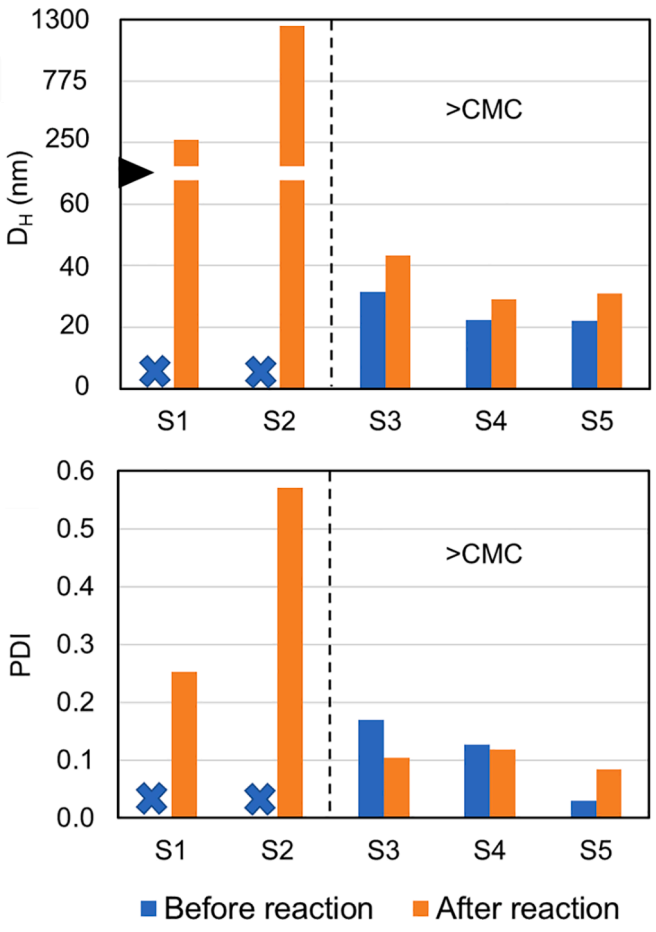

Fig. 1. PDA particle hydrodynamic diameter (D_H) and polydispersity index (PDI), measured via DLS for particles synthesised with increasing P-123 concentration. The dashed line indicates the critical micelle concentration (CMC). Samples, S1: 0 mg/ml, S2: 0.625 mg/ml (<CMC), S3: 2.5 mg/ml, S4, 5 mg/ml, S5: 20 mg/ml. The D_H axis is broken in two parts with different scales for better visualisation of the results. In S1 and S2, no micelles existed before the reaction. When micelles existed (S3, S4, S5) polydopamine particles were of similar size. All samples were prepared at ambient conditions (~20 °C, air atmosphere).

while with P-123 at a concentration below the CMC, >1000 nm diameter aggregates were found. In these preliminary experiments, darkening of the reaction solution, indicative of polydopamine formation, proceeded with a similar rate for all samples. Thus, no significant effect of the concentration of P-123 on polydopamine formation kinetics is expected.

Interestingly, polydopamine produced in presence of P-123 micelles did not visibly deposit on the reactor walls, as opposed to the other cases (<CMC concentration or no P-123 addition) where dark coloured film formation was observed on the magnetic stirrer and the glass vessel. Similar wall-coating suppression has been reported in the literature with the use of ionic surfactants during PDA synthesis [23]. However, with a smaller (compared to P-123) molecular weight non-ionic surfactant (Triton X-100) no suppression of film formation was observed [23]. This may be due to the lower molecular weight of PEG chain in Triton X-100 compared to P-123, which results to a lower amount of ether oxygen atoms available for hydrogen bonding in Triton X-100.

These findings verify the expected interaction between polydopamine and P-123 that modulates the nanoparticle growth. Based on the above, two possible pathways of size modulation via templating may be possible. Primary polydopamine aggregates formed by reacting monomers, attach on existing P-123 micelles via hydrogen bonding between the catechol groups and the ether oxygen atoms found in the hydrophilic PEG blocks of Pluronic P-123 on the micelle surface. PDA growth can then be directed by the initial PDA layer, since at low dopamine concentrations there are indications that growth of PDA films is favoured over creation of new particles [22,39]. Free (not forming micelles or adsorbed on a surface) P-123 molecules may also play a role in particle size modulation by attaching on the surface of PDA nanoparticles, limiting growth as reported for PEG [38]. Alternatively, the primary polydopamine aggregates are encapsulated in P-123 shortly after formation, limiting further growth as reported in [23] where ionic surfactants produced a similar effect. Particle growth can then proceed via continuous addition of PDA aggregates into the micelles, with free P-123 molecules being incorporated on the surface of the larger core. In any case, the existence of P-123 on the surface of the particles is likely, as it would explain the superior stability of P-123@PDA nanoparticles (no sedimentation even after weeks of storage at room temperature). An interaction between free P-123 and polydopamine is suspected for sample S2 shown in Fig. 1, where the particle size is significantly larger compared to synthesis without P-123.

In addition to hydrodynamic diameter, the UV–Vis absorption spectra of polydopamine nanoparticles produced in batch were obtained and were found virtually unchanged for all samples prepared with or without P-123, indicating that UV–Vis absorption can be used to monitor PDA synthesis regardless of its interaction with P-123 (see SI, section S2). It was observed that absorbance at higher wavelengths slightly decreased, while absorbance at lower wavelengths increased with increasing P-123 concentration; however, it is not clear whether this was just an effect of the polydopamine aggregate/particle size or alterations in its chemical structure.

3.2. Batch synthesis of P-123@PDA nanoparticles. Effect of temperature and O_2 pressure on polymerisation kinetics and particle size

The P-123@PDA system was used to study the kinetics of templated polydopamine nanoparticle formation as a function of temperature and oxygen concentration. A P-123 concentration of 5 mg/ml was used in all experiments. Another important parameter is the reaction temperature, affecting all stages of polydopamine synthesis, starting from the initial oxidation of dopamine and followed by the subsequent cyclisation, isomerisation and oligomerisation steps, as well as aggregation via intermolecular interactions. A recent study has demonstrated the effect of temperature in accelerating reaction kinetics showing a typical Arrhenius dependence [40]. It was shown that while a temperature increase up to 55 °C accelerated the reaction, heating was not enough to deplete dopamine within timescales that favour a continuous process (~1500 min were still required). In addition to the reaction rates, temperature also affects the balance of dissolved species in the reaction mixture, having an additional, indirect effect on the kinetics. In a dissolved oxygen-based process, for a given gas partial pressure the maximum dissolved oxygen concentration decreases with increase in temperature due to change in solubility. Thus, controlling the temperature alone is not enough to adequately accelerate polydopamine synthesis. While the reaction temperature is easily controlled, dissolved oxygen concentration is affected by other parameters (temperature, other solutes, pH) and thus the pressure of the oxygen atmosphere above the reactor was used instead as a more convenient control parameter.

The pH is also an important parameter which has been shown to affect the kinetics by controlling the rate of dopamine self-oxidation, with higher values accelerating this reaction step and affecting polydopamine particle size [16,41]. Hence, in this work the pH was kept constant at ~8.7 to promote high oxidation rates of dopamine ($pK_{a,\ dopamine} = \sim 9$) and isolate the effects of the other parameters. While Tris is typically the buffer of choice for polydopamine synthesis (and used in the present work), its buffering effect is affected by temperature, leading to approximately 1 pH unit change per 30 °C change in temperature [42]. To take the temperature dependency of pH into account, the solution pH was preadjusted when preparing the buffer solutions. A brief

evaluation of the effect of temperature on the pH of the Tris-buffered micellar solution used in the synthesis can be found in the SI, section S3.

A series of experiments to investigate the combined effect of reaction temperature and oxygen concentration (controlled via pressure) were conducted to cover a broad range, accounting for the system's technical limitations: from room temperature (20 °C) to 90 °C, which is close to the cloud point of Pluronic P-123 [43], and from 1 bar (atmospheric pressure) to 5 bar, which is the maximum recommended operating pressure for the pressure vessel used. Oxygen solubilities were calculated for a water – oxygen system via Henry's law and shown in the SI, section S4. It should be underlined that the pressure values of all the experiments refer to the pressure of the atmosphere above the reaction vessel, which after 60 min under a pressurised oxygen atmosphere contains mostly oxygen and water vapour. Preliminary experiments in an open vessel (air atmosphere, ~0.21 bar O_2) had shown slower UV–Vis absorption increase, especially at elevated temperatures, where the oxygen concentration decreases further due to reduction in solubility (see SI, section S5). Interestingly, when the synthesis was performed in an open vessel (exposed to air) and at high temperature (90 °C) no significant colour change was observed within the first 30 min after addition of dopamine.

The synthesis evolution over time was monitored by extracting small aliquots of the reaction mixture and measuring the UV–Vis absorption at 395 nm (characteristic of uncyclised chromophore building blocks produced by dopamine oxidation, such as dopamine-quinone), and at 620 nm (indole-5,6-quinone building blocks, the main building blocks of PDA) [16]. It should be noted that absorbance at 395 nm and 620 nm cannot be exclusively attributed to the aforementioned monomers, but

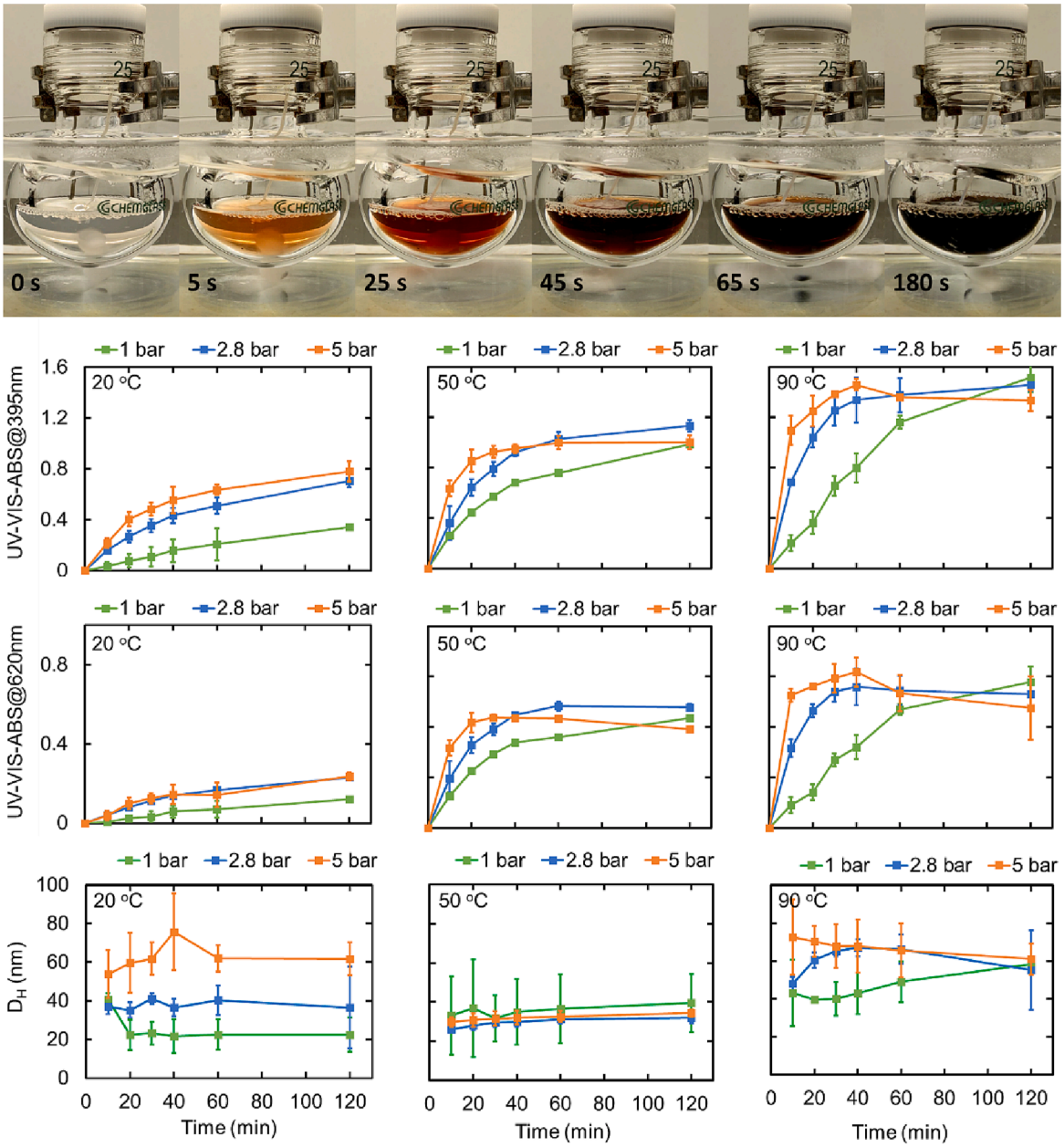

Fig. 2. Results from batch experiments performed to extract kinetic information. Top: Colour change of the reaction mixture during the first seconds of polydopamine synthesis in the pressurised batch reactor at 50 °C and 5 bar O_2. Middle: UV–Vis absorption over time of reacting polydopamine solutions at different reaction conditions (after 1/10 dilution of samples). The selected absorption wavelengths are representative of polydopamine building blocks formation. Bottom: Hydrodynamic diameter change over time as measured by DLS for different temperature and pressure conditions. Error bars represent maximum absolute error from duplicate experiments.

could also occur due to the formation of oligomers, and intermolecular interactions between the oligomers, such as π-π stacking [44]. Nevertheless, absorbance monitoring at these wavelengths can still provide particularly useful insights on how fast the reaction progresses, helping to identify the conditions that accelerate it. Fig. 2 shows the evolution of absorption over the first 2 h of the reaction for various temperature and pressure combinations. The evolution of the full spectrum for each case can be found in SI, section S6.

As shown in Fig. 2, both temperature increase and increase of pressure (and thus oxygen concentration) were found effective in accelerating polydopamine formation especially with a simultaneous increase of these parameters, which led to rapid colour change of the reactive mixture and plateauing in absorption within the 1st hour of reaction, even for conditions individually considered mild (e.g., 50 °C and 2.8 bar O_2). The higher absorption of 90 °C experiments was potentially related to the aggregation/assembly of PDA nanoparticles, since particle size may affect the absorbance via scattering effects.

One interesting observation is that in all intensified conditions cases ($P \geq 2.8$ bar O_2 and $T \geq 50$ °C), the absorption at 395 nm keeps rising throughout the synthesis duration, while the absorption at 620 nm starts dropping after a specific time point dependent on the conditions. This phenomenon can be attributed to high H_2O_2 concentration produced during the initial steps of dopamine oxidation [16], that potentially leads to oxidative degradation of indole-5,6-quinone building blocks (absorbing at 620 nm) to pyrrole-dicarboxylic acid [1]. Increasing oxygen concentration increases H_2O_2 production rate [16] and thus can accelerate the degradation rate, as indicated by the maximum in the absorption spectra over time (at 620 nm) and subsequent decline shown in Fig. 2. Such decline was found to be mitigated by bringing the reactive mixture to ambient conditions (oxygen desorption, cooling to room temperature) before a decrease in absorbance starts. Thus, when using intensified conditions for polydopamine nanoparticle synthesis, it is essential to tune the reaction time to benefit from the enhanced oxidation kinetics, while preventing degradation of the polydopamine product. Quenching the reaction via a free radical scavenger addition, such as mercaptoethanol or ascorbic acid is also expected to help prevent degradation, as it has been shown to be effective in inhibiting polydopamine free radicals [31].

Monitoring the hydrodynamic diameter during the reaction provided additional information on the reaction process, especially on how the particle size is modulated by the addition of P-123. The trends presented in Fig. 2 (bottom) show the dependency of particle size on reaction conditions, with higher pressures generally leading to larger particle sizes. The effect was less pronounced in all 50 °C cases (≥2.8 bar), where the particle size was tightly focused between 30 and 35 nm and the synthesis was characterised by very good reproducibility. This is an indication that the PDA particle size modulation is favoured by slightly elevated temperature. The polydispersity index (PDI) of these samples ($T = 50$ °C, $P \geq 2.8$ bar) was also low (<0.15) throughout the synthesis (shown in SI, section S7) as opposed to cases with slower kinetics where PDI started from higher values and decreased as the synthesis progressed.

Some potential explanations for these otherwise unexpected trends can be offered by revisiting the role of P-123 on particle size modulation. At low temperatures, P-123 molecules while mostly forming micelles, can also be freely dissolved in the aqueous solution and are subject to a dynamic equilibrium with the micelles [45]. Upon the start of PDA formation, such dissolved P-123 molecules may act as cross-linkers, assisting the formation of larger supramolecular structures (as discussed in section 3.1, for PDA formation with P-123 at < CMC concentration). Increasing the temperature to 50 °C, shifts the equilibrium towards micelle formation, reducing the amount of freely dissolved P-123 and subsequently the possibility of crosslinking events, resulting in improved nanoparticle size control despite the highly accelerated PDA formation kinetics. Increasing the temperature to 90 °C, further reduces the probability of hydrogen bonding [46] (and hence hydrophilicity), which could favour PDA aggregation over interaction with P-123 micelles. In addition, the temperature increase at 90 °C brings P-123 close to their cloud point [45], causing them to swell, which can also eventually lead to larger P-123@PDA nanoparticles. It should be noted that in our work, reaction of Tris with PDA was not considered important in the particle size modulation or kinetics of PDA formation due to the relatively low concentration of Tris [47]. However, the role of this reaction under intensified conditions might be more important than expected, and the use of non-reactive buffers might be worth further investigation.

In addition to the main sets of experiments, a brief, auxiliary kinetic study of pure polydopamine nanoparticle formation without using P-123 at 2.8 bar and 50 °C was conducted. This study showed an increase of UV–Vis absorbance at 395 nm and 620 nm similar to P-123@PDA synthesis at the same conditions (see SI, section S8), indicating similar PDA formation kinetics regardless of the existence of P-123. In contrast, while the hydrodynamic diameter of P-123@PDA nanoparticles was always confined to < 40 nm in these conditions, the size of pure PDA nanoparticles increased up to ~ 150 nm, reaching a plateau within 60 min. Interestingly, the size of pure PDA particles produced at intensified conditions (50 °C and 2.8 bar O_2) was smaller and more monodisperse (according to DLS obtained PDI) compared to the ambient synthesis (>250 nm as shown in Fig. 1). This trend agrees with a classic nucleation/growth scheme where higher initial nucleation rate leads to smaller final particle size [48]. This experiment verifies the role of P-123 as particle size modulator even in intensified conditions (i.e., without P-123 the nanoparticles become significantly larger even at a faster synthesis rate). More importantly, it demonstrates that accelerated polydopamine synthesis under intensified conditions is not a result of using the P-123 template and thus polydopamine synthesis using other templates could be accelerated using a similar approach.

3.3. Chemical and structural characterisation of polydopamine nanoparticles

While the main purpose of this work is the investigation of kinetics of polydopamine formation with the use of intensified conditions and the soft template-based synthesis, it is important to assess how the properties of the produced polydopamine nanoparticles are affected by the variation in synthesis conditions, and how they compare with a reference sample.

The P-123@PDA product stability was evaluated by obtaining the UV–Vis absorption spectra and particle size with DLS 24 h after the reaction mixture was returned to ambient conditions. In all cases, small changes in the UV–Vis absorption spectrum were observed (see SI, section S6), pointing to slow restructuring or degradation taking place, potentially involving oxidation of indole-5,6-quinone to pyrrole-carboxylic acids. Changes in particle size (see SI, section S9) can be associated with slow growth due to incomplete reaction in (20 °C, ≤ 2.8 bar) cases, while reduction of particle size at more intensified conditions indicates restructuring of polydopamine particles. It should be noted that all P-123@PDA samples, irrelevant of preparation conditions, exhibited good colloidal stability a week after preparation while stored at ambient conditions (no sedimentation occurred).

FTIR-ATR was used to identify the characteristic chemical moieties of P-123@PDA nanoparticles. All samples were separated and prepared for FTIR after 2 h reaction. The FTIR transmission spectra for various synthetic conditions are presented in Fig. 3a. The asymmetric double peak at 2365 and 2338 cm^{-1} corresponds to CO_2 due to imperfect purging of the measurement chamber [29]. The FTIR spectrum of all samples exhibits two broad bands which are commonly observed in polydopamine based materials. The broad band evident to all samples between 3600 and 3000 cm^{-1} is attributed to NH stretching of primary and secondary amine groups and OH stretching [49]. A second broad band can be found between 1730 and 1230 cm^{-1} with various small peaks protruding from it at 1630, 1595, 1555, 1510, 1458, 1393, 1373,

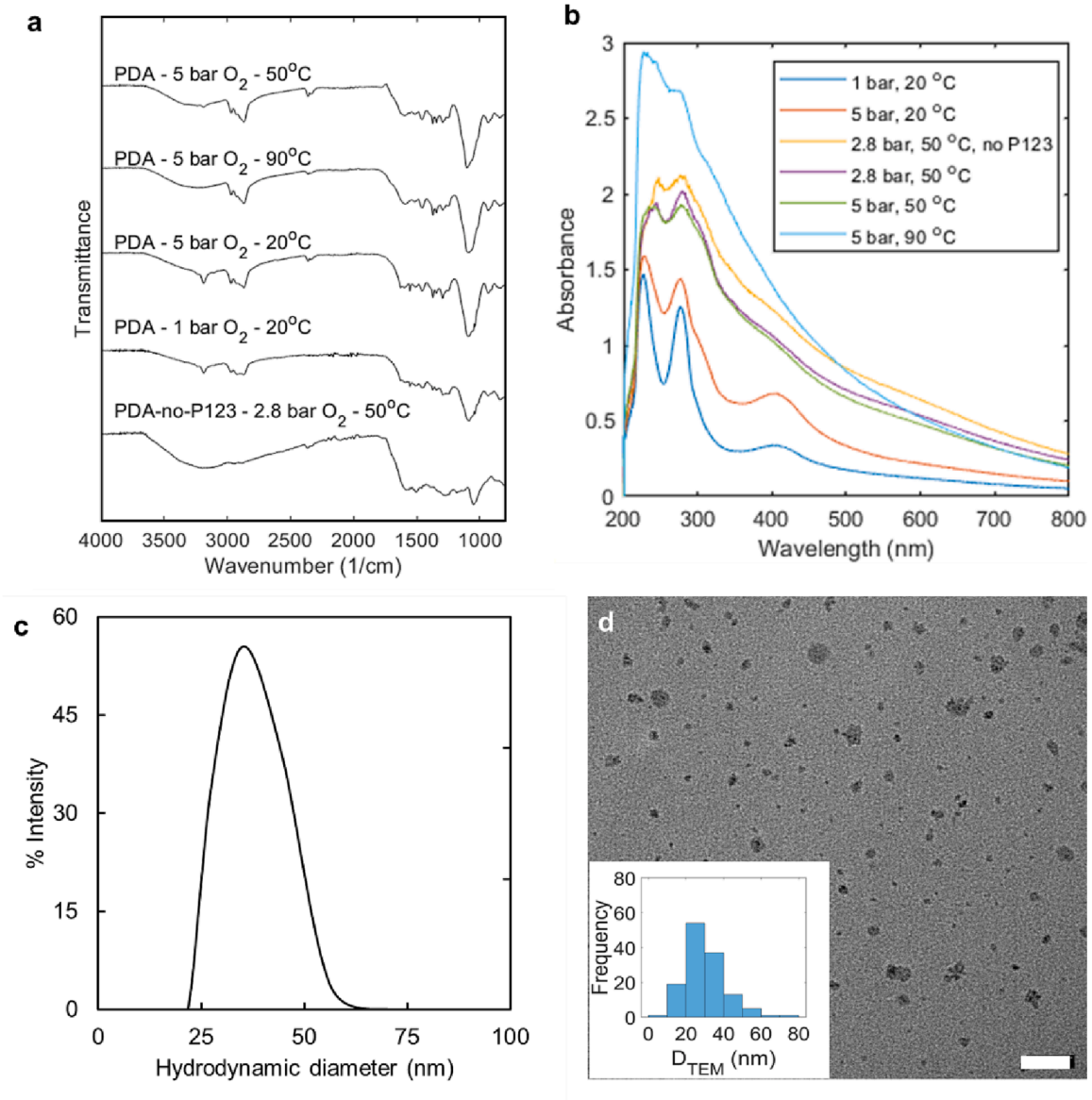

Fig. 3. Characterisation of P-123@PDA nanoparticles. a) ATR - FTIR spectra for P-123@PDA and pure PDA nanoparticles produced at various temperature and pressure conditions, shown above each graph. The samples were separated at 60 min of reaction. Spectra have been normalized with the minimum transmittance for easier comparison. b) Comparison of UV–Vis absorption spectra of P-123@PDA and pure PDA nanoparticles for various conditions obtained at 60 min of reaction. The spectrum of the 90 °C case was obtained with 1/20 dilution (instead of the 1/10 used in general) and then was multiplied by 2, to avoid spectrometer saturation. c) Particle size distribution obtained via DLS for the 50 °C, 5 bar sample (after 120 min reaction time). d) Representative TEM image and particle size distribution obtained via image analysis (of a sample produced in 5 bar and 50 °C). The scale bar represents 100 nm.

1340, 1292 and 1254 cm^{-1}. This band was attributed to stretching of the C=C bond in the aromatic rings, while the small protruding peaks are indicative of the heterogeneity of these aromatic rings' environment [50]. The protruding peaks in this band are different compared to the ones found in the pure polydopamine sample, which can be attributed to P-123 interaction with polydopamine. In addition, for the samples produced with P-123, a double asymmetric peak around 2874 cm^{-1} and 2970 cm^{-1} (C-C bond stretching) [49], match with the characteristic peaks of P-123 (see SI, section S10), indicating its incorporation in the polydopamine nanoparticles. Finally, a strong peak at 1100 cm^{-1}, found at every sample, characteristic of C-O stretching [49], can be attributed to abundant catechol groups which are expected in polydopamine, or due to incorporation of Tris in the final product. Among the P-123@PDA samples produced at various conditions, the most important differences in the FTIR spectra are a small sharp peak at 3190 cm^{-1} and a minor one at 1628 cm^{-1} which are predominant in the low temperature and high O_2 concentration conditions. These sharp peaks were attributed to primary amine units [49] and thus indicate the existence of uncyclised units in the polydopamine structure. This observation agrees with the hypothesis that increased O_2 concentration accelerates the formation of dopamine oxidation leading to fast accumulation of uncyclised oxidation products that may covalently bond to each other, or other PDA building blocks, and thus get incorporated into the polydopamine structure. Time-resolved FTIR (with sample collected every 10 min) was also performed for the 50 °C, 2.8 bar O_2 case of P-123@PDA showing that even under mildly intensified conditions, PDA was formed within the first 10 min with only minor changes happening afterwards (see SI, section S10).

Complementary to FTIR, Raman spectroscopy (@785 nm) was also used to analyse selected samples (see SI, section S11). The Raman spectra of P-123@PDA were characterised by broader peaks compared to pure PDA nanoparticles and by a broad shoulder at lower wave

numbers. The difference potentially corresponds to the interactions between PDA and P-123.

UV–Vis absorption (200–800 nm range) was used to evaluate the optical properties of P-123@PDA nanoparticles, while also providing some information on the existing building blocks (Fig. 3b). The spectra shown in Fig. 3b were obtained 1 h after the reaction start, with no new features (e.g., new peaks) arising after that point (refer to Fig. S8 in SI, section S6 for spectra evolution over time). In all cases, a broad spectrum with increasing intensity towards shorter wavelengths was obtained, characteristic for melanin-like materials [51]. Peaks at 230 and 280 nm found in the 20 °C cases are associated with dopamine [16], suggesting a degree of uncyclised dopamine embedded in the PDA structure. Shoulders at 300 nm found in all cases except the 20 °C, 1 bar sample, are (along with a peak at 275 nm found in all cases) characteristic of 5,6-dihydroxyindole, the main building block of polydopamine [16]. It should be noted that at lower temperatures the shoulder usually only appeared at the later stages of the reaction. Interestingly, in the 20 °C cases with elevated pressure, a significant peak at ~ 400 nm was obtained, which could be associated with the existence of intermediate dopamine-quinone [16] which absorbs at 395 nm and was expected to accumulate under high oxidant concentrations. The peak persists throughout the reaction to the final product (Fig. S8), indicating incorporation of the responsible building block in the final polydopamine structure. Finally, it should be noted that, as opposed to FTIR and Raman spectra, the UV–Vis spectra of PDA and P-123@PDA were very similar, both in features and intensity, indicating that despite PDA interaction with P123, the absorbance of the material is not altered (and thus UV–Vis monitoring can be a suitable method of evaluating PDA formation kinetics even in the presence of soft substrate).

The possibility of increased uncyclised amine building blocks amount at low temperatures and elevated pressure, indicated by the FTIR-ATR and UV–Vis spectroscopic analysis, could aid the explanation of the pressure dependency of particle size (shown in Fig. 2) at 20 °C. Assuming that increasing pressure (leading to higher dissolved oxygen concentration) increases the accumulation of uncyclised amine groups in the PDA structure, and that uncyclised amine groups can 1) act as cross linkers themselves (since their importance in polydopamine binding has been demonstrated by [15]) and 2) provide more groups capable of strong hydrogen bonding, then the increase of particle size at elevated pressure could be associated with enhanced crosslinking and/or hydrogen bonding by the uncyclised amine groups.

TEM analysis was used to evaluate the particle morphology and as a secondary means of measuring particle size. As shown in Fig. 3d, P-123@PDA nanoparticles produced at 50 °C and 5 bar appear well separated in the grid and are characterised by irregular shapes. The shape irregularity may be characteristic of small particle sizes and particle growth suppression, since formation of regular spherical particles, even under accelerated kinetics, occurs in the growth stage [50]. The particle size distribution, estimated by measurement of the maximum particle length in a representative particle population, was found comparable to DLS analysis albeit wider and shifted to smaller particle sizes with a mean of 29 nm and a standard deviation of 10.1 nm (compare with ~35 nm average particle size from DLS, shown in Fig. 3c). Discrepancies could be attributed to the fact that DLS measures hydrodynamic diameter and to the effect of nanoparticle drying during the grid preparation, which unlike crystalline nanoparticles, may be subject to deformation.

3.4. Flow synthesis of P-123@PDA nanoparticles in a millifluidic membrane reactor

The kinetic investigation of polydopamine formation in the presence of P123 micelles provided valuable kinetic information which enabled the rational design of a continuous production process. The continuous process was based on a co-axial membrane millifluidic reactor, which was designed to replicate the conditions of the batch process while allowing better control of the reaction environment, overcoming oxygen mass transfer limitations due to its small size.

CFD simulation (see SI, section S12) was used to model the oxygen pre-saturation section and evaluate the saturation achieved as a function of various operating conditions, taking into account the uncertainty of the surfactant solution mass transfer properties (such as diffusion coefficients). Based on a conservative approach (oxygen diffusion coefficient was assumed 4.5x lower in the surfactant solution compared to water), ~20 min of residence time of the micellar buffer in the presaturator would be adequate for complete saturation of the solution.

Informed by the kinetic experiments and the simulations, the pressure in the liquid phase was set to 5 bar to increase the solubility of oxygen in the reactive mixture, while the gas phase was pressurised (to 4.9 bar) to increase the oxygen partial pressure and consequently, the oxygen permeation rate through the membrane. The operation temperature was chosen as 50 °C, due to the tight particle size control demonstrated in the kinetic study. The residence time in the presaturator was set to 20 min, since the simulations showed complete saturation (under the chosen operation conditions), even with conservative assumptions for oxygen transport in the surfactant solution. The reactor residence time was restricted to 20 min, while at the outlet of the reactor excess oxygen was removed by collecting the sample to an ambient pressure vessel, to limit oxidative polydopamine degradation.

The reactor system was shown to successfully reproduce the results from the corresponding batch experiment and demonstrated stable operation for over 9x residence times producing a consistent product, monitored by DLS and UV–Vis spectroscopy (Fig. 4a). Furthermore, only small discrepancies in UV–Vis absorbance (±0.01 units at 395 nm) and hydrodynamic diameter (±1.4 nm or ± 4.5%) were observed in two independent runs of the synthesis. Although some fouling was found in the entrance section of the reactor after prolonged operation, the product seemed unaffected and reactor operation was not interrupted. After each use, the reactor was cleaned with 2 M NaOH solution, which removed the polydopamine coating from the capillary wall. The flow reactor product was characterised with UV–Vis spectroscopy, DLS, and FTIR, and compared with the batch reactor product prepared under similar conditions (at 20 min reaction time, equal to the continuous reactor residence time). The particle size distribution (Fig. 4b) (measured with DLS) obtained with the flow synthesis was narrow, similar to the corresponding batch. The UV–Vis absorbance (Fig. 4c) of the flow reactor product was slightly higher than of the corresponding batch, indicating slightly higher conversion within the given reaction time. Only subtle differences were observed, including a small shoulder at ~400 nm in the UV–Vis spectrum. In the FTIR spectrum (Fig. 4d), small sharp peaks were observed at 3190 cm^{-1} and 1628 cm^{-1} which were more pronounced compared to the corresponding batch (the difference in the double peak at 2365 and 2338 cm^{-1} can be attributed to differences in CO_2 atmosphere in the measurement chamber). Both these characteristics, according to analysis in section 3.3, indicate a slightly increased concentration of uncyclised monomers incorporated in the polydopamine particles. This effect could be attributed to the vastly enhanced oxygen mass transfer in the flow system that allowed faster replenishment of the consumed oxygen during the reaction stage, enabling faster accumulation of uncyclised oxidation products, as well as acceleration of subsequent oxidation stages, leading to higher overall (in all wavelengths) absorbance. In general, the product obtained from the flow synthesis was shown to be similar with the corresponding product obtained from the batch reactor, demonstrating the successful implementation of the flow system.

3.5. Photothermal properties of P-123@PDA nanoparticles

The photothermal heating of polydopamine samples under 808 nm NIR irradiation was measured using the setup described in section 2.5. Results of temperature increase with respect to time are presented in Fig. 5a for P-123@PDA nanoparticle dispersions produced batchwise at

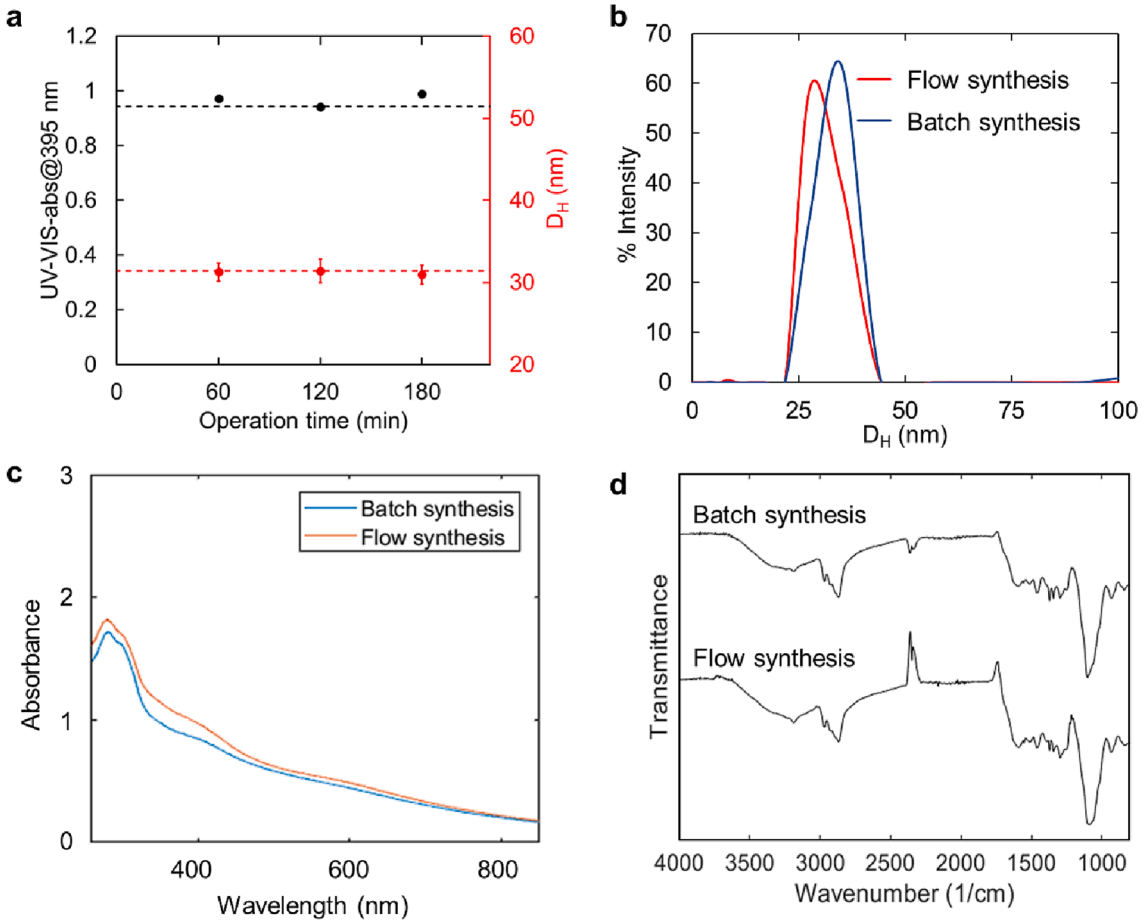

Fig. 4. Comparison of flow and batch synthesised P-123@PDA nanoparticles (batch synthesis with 20 min reaction time, equal to the flow reactor residence time, 50 °C, 5 bar) a) Demonstration of flow reactor polydopamine particle production over 3 h of operation and comparison with batch result for 20 min reaction time. The average values for batch synthesis are represented with dashed lines. Error bars indicate standard deviation between independent runs of flow synthesis. b) Particle size distribution obtained via DLS, c) UV–Vis absorbance spectra, d) FTIR spectra.

intensified conditions (50 °C, 5 bar O_2) within 20 and 60 min as well as P-123@PDA produced at ambient conditions in 24 h (all samples were produced in 26 ml batches). All the samples were measured at equal concentration of PDA in water, assuming full conversion of dopamine (the same amount of dopamine was used for the synthesis of each sample, and each sample was stored for 24 h before measurement to ensure full conversion, since this is the typical time required for reaction completion). In all cases the starting temperature was ~25.5 ± 0.2 °C, equal to room temperature and the experimental error of the measurements was ±1 °C, estimated by multiple measurements of the same sample. All samples exhibited similar performance indicating that heating capabilities of polydopamine nanoparticles are not affected by the intensified synthetic approach. Increasing the reaction time in intensified conditions from 20 min to 60 min showed a minor improvement of the photothermal effect which however, is within the experimental error. The P-123@PDA sample prepared at 50 °C, 5 bar, 20 min reaction time, underwent 3 cycles of photothermal heating and cooling showing good resistance of its properties to thermal strain and photobleaching (Fig. 5b). The effect of concentration was also briefly assessed (see SI, section S13). A heating plateau with increasing PDA concentration was found, indicating that at higher PDA concentrations, only a portion of nanoparticles absorb IR radiation at a given time (despite the active mixing) due to low penetration of the beam through the cuvette at high nanoparticle concentrations.

To put these results into context, assuming an average body temperature of 36 °C, a rapid increase of ~10 °C would bring the local temperature above 45 °C which would be sufficient for inducing hyperthermia conditions, eventually leading to effective treatment of cancer [39,52]. It should be noted that in none of the cases studied in our work the temperature reached a plateau, and thus increased laser exposure could lead to even higher temperatures. The relatively small size of the nanoparticles (<40 nm) may also bring additional advantages in terms of increased cell uptake, or increased probability to cross the blood brain barrier [53].

Comparing with literature, [54] achieved a temperature increase of 25 °C at 0.2 mg/ml of pure polydopamine nanoparticles (prepared without any surfactant), at 2 W/cm^2 laser fluence, in 5 min, while [55] obtained a temperature increase of 15 °C at 0.2 mg/ml of mesoporous polydopamine core and polydopamine shell particles (prepared via a templated synthesis using Pluronic F-127) at 1 W/cm^2 laser fluence, in 5 min. In the present work under similar conditions (0.154 mg/ml, 1.77 W/cm^2 laser fluence, 5 min irradiation), a temperature increase of 6 °C was observed (see SI, section S13). It must be noted though that direct comparison with the literature is difficult due to differences in the measurement procedure. For example, [54] placed the thermocouple inside the cuvette, resulting to a 3 °C measured temperature rise of pure water in 5 min, while in the present work the thermocouple was placed outside, but in direct contact with the quartz cuvette containing the sample, resulting in a measured temperature increase of water (combined with the energy input from stirring) of 1.6 °C, after 5 min of laser irradiation.

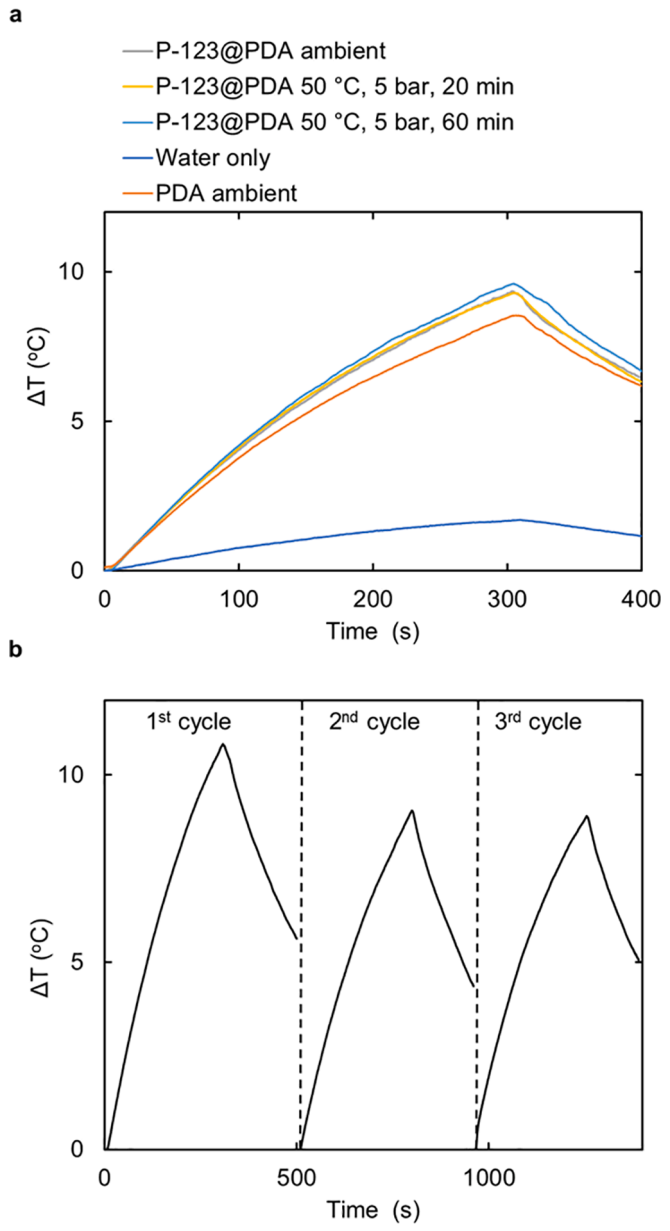

Fig. 5. Photothermal heating assessment of PDA nanoparticles. a) Comparison of samples prepared at different conditions (batch, dopamine concentration 0.769 mg/ml), b) Multiple heating and cooling cycles of "P-123@PDA 50 °C, 5 bar, 20 min" sample (0.769 mg/ml). Part of heating in each sample is attributed to the magnetic stirring and the laser irradiation absorbed by water. The initial temperature was 25.5 ± 0.2 °C. In all cases the laser power was set to the minimum setting, 0.5 W.

4. Conclusions

This work demonstrated the design of a continuous process for polydopamine nanoparticle synthesis for photothermal applications, starting from a soft template for particle size control, performing an extensive investigation of the reaction kinetics under intensified conditions and their effect on the product properties, and ultimately utilising these findings for the design of a continuous manufacturing process.

The addition of Pluronic P-123 (at small concentrations above its critical micelle concentration), used for the first time as a modulator of polydopamine synthesis enabled the restriction of particle size at the sub-50 nm range, which is not easily achievable via non-templated synthesis. In addition, in the presence of P-123 micelles the deposition of PDA films on reactor vessel components was greatly reduced in favour of small nanoparticle production. Potential explanations of this behaviour include: the selective growth of polydopamine on P-123 micelles, which is suggested by the size similarity between the PDA nanoparticles and the P-123 micelles, and incorporation of P-123 in polydopamine particles as indicated by FTIR, or the suppression of polydopamine nanoparticle aggregation into larger particles and uncontrollable growth by attachment of P-123 molecules on growing PDA nanoparticles which promote repulsive interactions. Although additional research is required to verify the exact role of P-123 micelles on polydopamine nanoparticle size control, their effectiveness has been successfully demonstrated.

The P-123@PDA system was used for polydopamine formation kinetics investigation as a function of reaction temperature and oxygen concentration, which was controlled via the pressure of oxygen atmosphere. Adjusting the reaction temperature and using pressurized pure oxygen allows controlling the kinetics of polydopamine formation by modifying the rates of the reaction steps leading from dopamine to 5,6-dihydroxyindole and indole-5,6-quinone, the primary building blocks of polydopamine. Increased pressure led to higher oxygen concentration, which accelerated the oxidative steps required to initiate dopamine oxidation and oxidation of intermediate species by increasing the concentration of free radicals. Increased temperature accelerated all the intermediate reaction steps, including cyclisation and isomerisation, as well as monomer coupling, leading to faster formation of polydopamine. Since increasing the temperature results in reduced oxygen solubility, a simultaneous increase of both oxygen pressure and reaction temperature was shown to be essential to accelerate the reaction rate. Prolonged residence times in intensified conditions were shown to promote polydopamine degradation, potentially via indole-5,6-quinone oxidation, underlining the importance of tuning the reaction time.

The evolution of P-123@PDA hydrodynamic diameter during the kinetic experiments led to the identification of an important interplay not only between the reaction conditions and the produced polydopamine building blocks, but also between the interactions of PDA with the nano-substrate P-123 that affects the particle size in otherwise unexpected ways. At room temperature (20 °C) and elevated pressure, a combination of increased uncyclised amine building blocks in the PDA structure along with the existence of non-micellar surfactant in solution may be responsible for extensive crosslinking, potentially via hydrogen bonding, that eventually led to larger particle sizes. At slightly elevated temperatures, the increased micellisation, the reduction of uncyclised amine group content, or a combination of both led to tight particle size control close to that observed at ambient conditions, but with accelerated kinetics. Finally at high temperatures (90 °C) despite the rapid kinetics, the particle size control was less effective, potentially due to the weakening of intermolecular interactions and particle size dependency of P-123 micelles as they approach the cloud point.

The kinetics acceleration with temperature and oxygen pressure combination was observed even without the use of P-123 as particle size modulator. However, the particle size at intensified conditions was significantly reduced compared to ambient conditions, which could be explained by an increased rate of nucleation under faster kinetics. This offers the potential of using the reaction conditions, as a means of controlling particle size of pure polydopamine nanoparticles, and polydopamine coatings on other nanosized templates.

The data gathered from the kinetic experiments informed the transition from a batch to a continuous P-123@PDA nanoparticle production process by identifying the optimal operating conditions and reaction time to accelerate PDA production without degradation. The continuous process was based on a millifluidic co-axial membrane reactor that allows more efficient oxygen supply in the reactive mixture compared to batch. The continuous process was demonstrated to successfully replicate the target product from the batch and operate continuously for 9x residence times without decline in product quality. The addition of P-

123 significantly mitigated fouling in the flow reactor allowing prolonged operation.

Finally, testing the photothermal heating capability of P-123@PDA nanoparticles under IR@808 nm irradiation demonstrated adequate heating to surpass the hyperthermia barrier within 5 min of irradiation. The relatively small size, combined with the proven photothermal properties of polydopamine, makes these nanoparticles attractive towards the development of photothermal cancer therapies.

Declaration of Competing Interest

The authors declare that they have no known competing financial interests or personal relationships that could have appeared to influence the work reported in this paper.

Data availability

Data will be made available on request.

Acknowledgments

We thank Dr. Daniel Hauser for useful discussions regarding polydopamine chemistry and applications. We thank Prof. Nikolitsa Nomikou for providing equipment used in the photothermal measurements. We thank the EPSRC (EP/M015157/1) through the Manufacturing Advanced Functional Materials (MAFuMa) scheme for financial support. Georgios Gkogkos is grateful to the Hugh Walter Stern PhD studentship for his funding.

Appendix A. Supplementary data

Supplementary data to this article can be found online at https://doi.org/10.1016/j.cej.2023.143350.

References

[1] J.H. Ryu, P.B. Messersmith, H. Lee, Polydopamine surface chemistry: a decade of discovery, ACS Appl. Mater. Interfaces 10 (2018) 7523–7540, https://doi.org/10.1021/acsami.7b19865.
[2] P. Yang, F. Zhu, Z. Zhang, Y. Cheng, Z. Wang, Y. Li, Stimuli-responsive polydopamine-based smart materials, Chem. Soc. Rev. 50 (2021) 8319–8343, https://doi.org/10.1039/D1CS00374G.
[3] R. Batul, T. Tamanna, A. Khaliq, A. Yu, Recent progress in the biomedical applications of polydopamine nanostructures, Biomater. Sci. 5 (2017) 1204–1229, https://doi.org/10.1039/c7bm00187h.
[4] I. Singh, G. Dhawan, S. Gupta, P. Kumar, Recent advances in a polydopamine-mediated antimicrobial adhesion system, Front. Microbiol. 11 (2021) 3326, https://doi.org/10.3389/fmicb.2020.607099.
[5] M. Battaglini, A. Marino, A. Carmignani, C. Tapeinos, V. Cauda, A. Ancona, N. Garino, V. Vighetto, G. La Rosa, E. Sinibaldi, G. Ciofani, Polydopamine nanoparticles as an organic and biodegradable multitasking tool for neuroprotection and remote neuronal stimulation, ACS Appl. Mater. Interfaces 12 (2020) 35782–35798, https://doi.org/10.1021/ACSAMI.0C05497/ASSET/IMAGES/MEDIUM/AM0C05497_M011.GIF.
[6] A. Carmignani, M. Battaglini, E. Sinibaldi, A. Marino, V. Vighetto, V. Cauda, G. Ciofani, In vitro and ex vivo investigation of the effects of polydopamine nanoparticle size on their antioxidant and photothermal properties: implications for biomedical applications, ACS Appl. Nano Mater. 5 (2022) 1702–1713, https://doi.org/10.1021/acsanm.1c04536.
[7] H. Li, J. Xi, A.G. Donaghue, J. Keum, Y. Zhao, K. An, E.R. McKenzie, F. Ren, Synthesis and catalytic performance of polydopamine supported metal nanoparticles, Sci. Rep. 10 (2020) 1–7, https://doi.org/10.1038/s41598-020-67458-9.
[8] Á. Molnár, Polydopamine – its prolific use as catalyst and support material, ChemCatChem 12 (2020) 2649–2689, https://doi.org/10.1002/cctc.201902125.
[9] K. Qu, Y. Wang, A. Vasileff, Y. Jiao, H. Chen, Y. Zheng, Polydopamine-inspired nanomaterials for energy conversion and storage, J. Mater. Chem. A 6 (2018) 21827–21846, https://doi.org/10.1039/C8TA05245J.
[10] D. Aguilar-Ferrer, J. Szewczyk, E. Coy, Recent developments in polydopamine-based photocatalytic nanocomposites for energy production: physico-chemical properties and perspectives, Catal. Today 397–399 (2022) 316–349, https://doi.org/10.1016/j.cattod.2021.08.016.
[11] M. D'ischia, A. Napolitano, V. Ball, C.-T. Chen, M.J. Buehler, Polydopamine and eumelanin: from structure–property relationships to a unified tailoring strategy, 47 (2014) 3541-3550. https://doi.org/10.1021/ar500273y.
[12] J. Liebscher, Chemistry of polydopamine – scope, variation, and limitation, Eur. J. Org. Chem. (2019) 4976–4994, https://doi.org/10.1002/ejoc.201900445.
[13] M. Wu, T. Wang, L. Müller, F.A. Müller, Adjustable synthesis of polydopamine nanospheres and their nucleation and growth, Colloids Surf., A Physicochem. Eng. Asp. 603 (2020), 125196, https://doi.org/10.1016/J.COLSURFA.2020.125196.
[14] V. Ball, Polydopamine nanomaterials: Recent advances in synthesis methods and applications, Front. Bioeng. Biotechnol. 6 (2018) 109, https://doi.org/10.3389/FBIOE.2018.00109.
[15] M.L. Alfieri, L. Panzella, S.L. Oscurato, M. Salvatore, R. Avolio, M.E. Errico, P. Maddalena, A. Napolitano, M. d'Ischia, The chemistry of polydopamine film formation: the amine-quinone interplay, Biomimetics 3 (2018) 26, https://doi.org/10.3390/biomimetics3030026.
[16] M. Salomäki, L. Marttila, H. Kivelä, T. Ouvinen, J. Lukkari, Effects of pH and oxidants on the first steps of polydopamine formation: a thermodynamic approach, J. Phys. Chem. B 122 (2018) 6314–6327, https://doi.org/10.1021/acs.jpcb.8b02304.
[17] A.M. Jaramillo, R. Barrera-Gutiérrez, M.T. Cortés, Synthesis, follow-up, and characterization of polydopamine-like coatings departing from micromolar dopamine- o-quinone precursor concentrations, ACS Omega 5 (2020) 15016–15027, https://doi.org/10.1021/acsomega.0c00676.
[18] V. Ball, D. Del Frari, V. Toniazzo, D. Ruch, Kinetics of polydopamine film deposition as a function of pH and dopamine concentration: insights in the polydopamine deposition mechanism, J. Colloid Interface Sci. 386 (2012) 366–372, https://doi.org/10.1016/j.jcis.2012.07.030.
[19] H.Q. Tran, M. Bhave, G. Xu, C. Sun, A. Yu, Synthesis of polydopamine hollow capsules via a polydopamine mediated silica water dissolution process and its application for enzyme encapsulation, Front. Chem. 7 (2019) 468, https://doi.org/10.3389/fchem.2019.00468.
[20] M. Zhu, Y. Shi, Y. Shan, J. Guo, X. Song, Y. Wu, M. Wu, Y. Lu, W. Chen, X. Xu, L. Tang, Recent developments in mesoporous polydopamine-derived nanoplatforms for cancer theranostics, J. Nanobiotechnol. 19 (2021) 1–22, https://doi.org/10.1186/s12951-021-01131-9.
[21] M. Maruthapandi, A. Saravanan, J.H.T. Luong, A. Gedanken, Polydopamine decorated carbon dots nanocomposite as an effective adsorbent for phenolic compounds, J. Appl. Polym. Sci. 139 (2022) 1–13, https://doi.org/10.1002/app.51769.
[22] B. Fei, B. Qian, Z. Yang, R. Wang, W.C. Liu, C.L. Mak, J.H. Xin, Coating carbon nanotubes by spontaneous oxidative polymerization of dopamine, Carbon 46 (2008) 1795–1797, https://doi.org/10.1016/j.carbon.2008.06.049.
[23] F. Ponzio, P. Bertani, V. Ball, Role of surfactants in the control of dopamine-eumelanin particle size and in the inhibition of film deposition at solid-liquid interfaces, J. Colloid Interface Sci. 431 (2014) 176–179, https://doi.org/10.1016/j.jcis.2014.06.025.
[24] F. Chen, Y. Xing, Z. Wang, X. Zheng, J. Zhang, K. Cai, Nanoscale polydopamine (PDA) meets π-π interactions: an interface-directed coassembly approach for mesoporous nanoparticles, Langmuir 32 (2016) 12119–12128, https://doi.org/10.1021/acs.langmuir.6b03294.
[25] B.Y. Guan, S.L. Zhang, X.W. Lou, Realization of walnut-shaped particles with macro-/mesoporous open channels through pore architecture manipulation and their use in electrocatalytic oxygen reduction, Angew. Chem. Int. Ed. 57 (2018) 6176–6180, https://doi.org/10.1002/ANIE.201801876.
[26] F. Ponzio, J. Barthès, J. Bour, M. Michel, P. Bertani, J. Hemmerlé, M. D'Ischia, V. Ball, Oxidant control of polydopamine surface chemistry in acids: a mechanism-based entry to superhydrophilic-superoleophobic coatings, Chem. Mater. 28 (2016) 4697–4705, https://doi.org/10.1021/acs.chemmater.6b01587.
[27] J. Li, M.A. Baird, M.A. Davis, W. Tai, L.S. Zweifel, K.M.A. Waldorf, M. Gale, L. Rajagopal, R.H. Pierce, X. Gao, Dramatic enhancement of the detection limits of bioassays via ultrafast deposition of polydopamine, Nat. Biomed. Eng. 1 (2017) 1–12, https://doi.org/10.1038/s41551-017-0082.
[28] Q. Li, T. Zhang, J. Chen, W. Ji, Y. Wei, In situ synthesis of fluorescent polydopamine polymer dots based on Fenton reaction for a multi-sensing platform, J. Mater. Chem. B 9 (2021) 5503–5513, https://doi.org/10.1039/d1tb00764e.
[29] E.S. Bronze-Uhle, J.V. Paulin, M. Piacenti-Silva, C. Battocchio, M.L.M. Rocco, C.F. de O. Graeff, Melanin synthesis under oxygen pressure, Polym. Int. 65 (2016) 1339–1346, https://doi.org/10.1002/pi.5185.
[30] P. Zhou, Y.i. Deng, B. Lyu, R. Zhang, H. Zhang, H. Ma, Y. Lyu, S. Wei, J. Zheng, Rapidly-deposited polydopamine coating via high temperature and vigorous stirring: formation, characterization and biofunctional evaluation, PLoS One 9 (11) (2014) e113087, https://doi.org/10.1371/journal.pone.0113087.
[31] X. Du, L. Li, F. Behboodi-Sadabad, A. Welle, J. Li, S. Heissler, H. Zhang, N. Plumeré, P.A. Levkin, Bio-inspired strategy for controlled dopamine polymerization in basic solutions, Polym. Chem. 8 (2017) 2145–2151, https://doi.org/10.1039/c7py00051k.
[32] X. Du, L. Li, J. Li, C. Yang, N. Frenkel, A. Welle, S. Heissler, A. Nefedov, M. Grunze, P.A. Levkin, UV-triggered dopamine polymerization: Control of polymerization, surface coating, and photopatterning, Adv. Mater. 26 (2014) 8029–8033, https://doi.org/10.1002/adma.201403709.
[33] M. Lee, S.H. Lee, I.K. Oh, H. Lee, Microwave-accelerated rapid, chemical oxidant-free, material-independent surface chemistry of poly(dopamine), Small 13 (2017) 1600443, https://doi.org/10.1002/smll.201600443.
[34] A. Cihanoğlu, J.D. Schiffman, S.A. Altinkaya, Ultrasound-assisted dopamine polymerization: rapid and oxidizing agent-free polydopamine coatings on membrane surfaces, Chem. Commun. 57 (2021) 13740–13743, https://doi.org/10.1039/d1cc05960b.
[35] G.B. Hwang, G. Wu, J. Shin, L. Panariello, V. Sebastian, K. Karu, E. Allan, A. Gavriilidis, I.P. Parkin, Continuous single-phase synthesis of [$Au_{25}(Cys)_{18}$]

nanoclusters and their photobactericidal enhancement, ACS Appl. Mater. Interfaces 12 (2020) 49021–49029, https://doi.org/10.1021/acsami.0c07691.
[36] L. Yang, K.F. Jensen, Mass transport and reactions in the tube-in-tube reactor, Org. Process Res. Dev. 17 (2013) 927–933, https://doi.org/10.1021/op400085a.
[37] Z. He, P. Alexandridis, Micellization thermodynamics of pluronic P123 (EO20PO70EO20) amphiphilic block copolymer in aqueous ethylammonium nitrate (EAN) solutions, Polymers (Basel) 10 (1) (2018) 32, https://doi.org/10.3390/polym10010032.
[38] S.-C. Chou, W.-A. Chung, T.-L. Fan, Y. Dordi, J. Koike, P.-W. Wu, Polydopamine and its composite film as an adhesion layer for Cu electroless deposition on SiO_2, J. Electrochem. Soc. 167 (4) (2020), 042507, https://doi.org/10.1149/1945-7111/ab7aa2.
[39] I. Zmerli, J.-P. Michel, A. Makky, Multifunctional polydopamine-based nanoparticles: Synthesis, physico-chemical properties and applications for bimodal photothermal/photodynamic therapy of cancer, Multifunct. Mater. 4 (2) (2021) 022001, https://doi.org/10.1088/2399-7532/abf0fa.
[40] J.C. García-Mayorga, H.C. Rosu, A.B. Jasso-Salcedo, V.A. Escobar-Barrios, Kinetic study of polydopamine sphere synthesis using tris: Relationship between synthesis conditions and final properties, RSC Adv. 13 (2023) 5081–5095, https://doi.org/10.1039/D2RA06669F.
[41] C.C. Ho, S.J. Ding, The pH-controlled nanoparticles size of polydopamine for anti-cancer drug delivery, J. Mater. Sci. - Mater. Med. 24 (2013) 2381–2390, https://doi.org/10.1007/s10856-013-4994-2.
[42] K. Reineke, A. Mathys, D. Knorr, Shift of pH-value during thermal treatments in buffer solutions and selected foods, Int. J. Food Prop. 14 (2011) 870–881, https://doi.org/10.1080/10942910903456978.
[43] R. Ganguly, M. Kumbhakar, V.K. Aswal, Time dependent growth of the block copolymer P123 micelles near cloud point: Employing heat cycling as a tool to form kinetically stable wormlike micelles, J. Phys. Chem. B 113 (2009) 9441–9446, https://doi.org/10.1021/jp900535f.
[44] D. Tuna, A. Udvarhelyi, A.L. Sobolewski, W. Domcke, T. Domratcheva, Onset of the electronic absorption spectra of isolated and π-stacked oligomers of 5,6-dihydroxyindole: an ab initio study of the building blocks of eumelanin, J. Phys. Chem. B 120 (2016) 3493–3502, https://doi.org/10.1021/acs.jpcb.6b01793.
[45] V. Singh, P. Khullar, N.P. Dave, N. Kaur, Micelles, mixed micelles, and applications of polyoxypropylene (ppo)-polyoxyethylene (peo)-polyoxypropylene (ppo) triblock polymers, Int. J. Ind. Chem. 4 (2013) 12, https://doi.org/10.1186/2228-5547-4-12.
[46] B.S. Lee, Pressure, temperature and concentration effects on hydrogen bonding in poly(ethylene oxide) aqueous solution, J. Mol. Liq. 262 (2018) 527–532, https://doi.org/10.1016/j.molliq.2018.04.127.
[47] N.F. Della Vecchia, A. Luchini, A. Napolitano, G. D'Errico, G. Vitiello, N. Szekely, M. d'Ischia, L. Paduano, Tris buffer modulates polydopamine growth, aggregation, and paramagnetic properties, Langmuir 30 (32) (2014) 9811–9818, https://doi.org/10.1021/la501560z.
[48] K.Y. Ju, Y. Lee, S. Lee, S.B. Park, J.K. Lee, Bioinspired polymerization of dopamine to generate melanin-like nanoparticles having an excellent free-radical-scavenging property, Biomacromolecules 12 (2011) 625–632, https://doi.org/10.1021/bm101281b.
[49] R.M. Silverstein, F.X. Webster, D.J. Kiemle, Spectrometric Identification of Organic Compounds, 7th ed., John Wiley & Sons Inc, Hoboken, NJ, 2005.
[50] S. Wang, S. Wannasarit, P. Figueiredo, J. Li, A. Correia, B. Xia, R. Wiwattanapatapee, J. Hirvonen, D. Liu, W. Li, H.A. Santos, Superfast and controllable microfluidic inking of anti-inflammatory melanin-like nanoparticles inspired by cephalopods, Mater. Horiz. 7 (2020) 1573–1580, https://doi.org/10.1039/d0mh00014k.
[51] M.L. Tran, B.J. Powell, P. Meredith, Chemical and structural disorder in eumelanins: a possible explanation for broadband absorbance, Biophys. J. 90 (2006) 743–752, https://doi.org/10.1529/biophysj.105.069096.
[52] D. Jaque, L. Martínez Maestro, B. Del Rosal, P. Haro-Gonzalez, A. Benayas, J. L. Plaza, E. Martín Rodríguez, J. García Solé, Nanoparticles for photothermal therapies, Nanoscale 6 (2014) 9494–9530, https://doi.org/10.1039/c4nr00708e.
[53] J. Dolai, K. Mandal, N.R. Jana, Nanoparticle size effects in biomedical applications, ACS Appl. Nano Mater. 4 (2021) 6471–6496, https://doi.org/10.1021/acsanm.1c00987.
[54] Y. Liu, K. Ai, J. Liu, M. Deng, Y. He, L. Lu, Dopamine-melanin colloidal nanospheres: an efficient near-infrared photothermal therapeutic agent for in vivo cancer therapy, Adv. Mater. 25 (2013) 1353–1359, https://doi.org/10.1002/adma.201204683.
[55] H. Chen, H. Chen, Y. Wang, Y. Bai, P. Yuan, Z. Che, L. Zhang, A novel self-coated polydopamine nanoparticle for synergistic photothermal-chemotherapy, Colloids Surf. B Biointerfaces 200 (2021), 111596, https://doi.org/10.1016/j.colsurfb.2021.111596.